
Article:
Yan, L., Hao, J., Zhang, Z. et al. (2023) Curvature Estimation of Soft Grippers Based on a Novel High-Stretchable Strain Sensor with Worm-Surface-like Microstructures. IEEE Sensors Journal. ISSN: 1530-437X

https://doi.org/10.1109/jsen.2023.3343370

Curvature Estimation of Soft Grippers Based on a Novel High-Stretchable Strain Sensor with Worm-Surface-like Microstructures

Lin Yan, Jianxiong Hao, Zhiqiang Zhang, Rui Liu, Hui Yang, Chaoyang Shi

***Abstract*—This paper presents a high-stretchable strain sensor based on the worm-surface-like microstructures and the principle of resistance sensing to estimate the curvature information of the soft pneumatic gripper with a large bending angle. The proposed sensor comprises a central viscoelastic fiber with worm-surface-like microstructures made of Ecoflex-10 silicone and an outside conductive layer of Carbon Black (CB) powder. The microstructures are generated by a 3D printing customized mold, and they can effectively increase the surface area and adhesion energy of the viscoelastic fiber so that more conductive powder can be adsorbed. Therefore, the proposed sensor produces lower resistance in the initial state and generates a more stable circuit connection and electrical signal transmission in the extremely stretched state, significantly improving the sensor sensitivity. Meanwhile, the microstructures can reduce the surface strain of the viscoelastic fiber during stretching and further increase the sensor's measurement range. The flexibility improvement of the proposed sensor brought by the microstructures can additionally reduce the required tension for achieving equivalent deformation, reducing the impact on the motion of the measured soft grippers. The electrical performances of the high-stretchable strain sensor have been characterized, and it can reach an excellent strain range of up to 500% with a gauge factor of 206.6. The prototyped strain sensor has been integrated on a soft pneumatic gripper's outside surface and well reflected the unknown objects' curvature radius with an average error of 4.07% during the grasping experiments.**

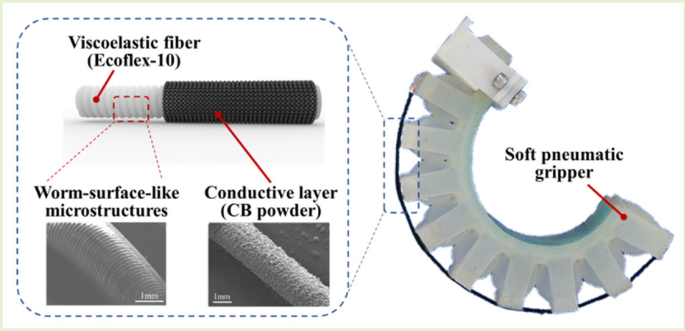

***Index Terms*—Flexible strain sensor, Microstructures, Soft pneumatic gripper, Shape sensing, Curvature estimation.**

I. Introduction

Soft robots made of hyperelastic materials have attracted significant attention due to their compliant, flexible, and deformable structures and excellent adaptability [1, 2]. Unlike traditional rigid robots, soft robots can adapt to complex and unpredictable environments, making them suitable for a wide range of applications, such as flexible rehabilitation robots [3, 4], soft surgical robots [5, 6], and various adaptive grippers [7, 8]. In these applications, it is essential to incorporate shape feedback through shape estimation techniques into the control process to achieve perception of soft robot shapes and further enhance control accuracy. Nevertheless, soft robots encounter obstacles in addressing nonlinear behaviors, evident hysteresis, and the absence of dependable, wide-ranging force and shape-sensing methodologies. These factors all impede the achievement of shape-sensing capabilities in soft robotic systems [9]. Strain sensors play a vital role in shape sensing, as they effectively capture and transmit the deformation of soft robots utilizing an electrical signal response. However, soft robots are capable of generating strains up to 200%-700% [10], which imposes greater demands on the stretchability of strain sensors.

Traditional rigid strain sensors are not able to fit the soft and deformable body of soft robots due to their high stiffness and poor stretchability [11, 12]. Many of them even impede the motions of soft robots after integration. In contrast, flexible strain sensors can be applied to soft robots due to their flexibility, ductility, and biocompatibility. The common flexible strain sensors mainly include fiber optic sensors [13, 14], capacitive sensors [15-18], resistive sensors [19-22], and so on.

Fiber optic sensors usually consist of an emitter, a receiver, and an intermediary [9]. When the fiber optic undergoes tensile deformation, the refractive index or intensity of light changes, so the fiber optic sensor can measure the deformation based on the change in these signals [23, 24]. Fiber optic sensors exhibit inherent electrical safety, immunity to electromagnetic interference, and compact size [25]. However, their application

Manuscript received on Sep 29, 2022. This work is supported in part by National Natural Science Foundation of China under Grant 62211530111, Grant 61973231, Grant 92148201 and Royal Society under IEC\NSFC\211360. L. Yan and J. Hao contribute equally to this work. Corresponding author: C. Shi and H. Yang (e-mail: chaoyang.shi@tju.edu.cn ; yanghui2018@tju.edu.cn).

L. Yan, J. Hao and C. Shi are with Key Laboratory of Mechanism Theory and Equipment Design of Ministry of Education, School of Mechanical Engineering, Tianjin University, Tianjin, 300072, China. Z. Zhang is with School of Electronic and Electrical Engineering, University of Leeds, Leeds, LS2 9JT, UK. H. Yang is with Tianjin Key Laboratory of Molecular Optoelectronic Sciences, Department of Chemistry School of Science, Tianjin University, Tianjin 300072, China. This work is also supported by International Institute for Innovative Design and Intelligent Manufacturing of Tianjin University in Zhejiang, Shaoxing 312000, CN.

in soft robots is limited by the complexity and high expense of measurement equipment [26] as well as the low stretchability and stiffness of traditional optical fibers.

Capacitive strain sensors typically consist of a pair of electrode plates and a separated flexible dielectric layer sandwiched between them [27]. The measured strain changes the distance between the electrode plates, leading to variations in the capacitance value. Capacitive strain sensors demonstrate the advantages of low power consumption, robust cycling stability, and low hysteresis. They are commonly utilized to measure the vertical pressure/strain information instead of the axial tensile strain [17]. However, they possess nonlinear sensitivity to strain, a limited operating range for strain measurement, and are vulnerable to environmental interferences. Therefore, it is necessary to consider environmental factors such as temperature, humidity, and magnetic fields, limiting their potential applications in soft robots.

Resistive strain sensors typically comprise a conductive sensing layer and a flexible substrate [28-30]. When the composite structure is stretched, the sensor undergoes deformation, leading to a change in resistance with applied strain. Once the strain is released, the sensor reverts to its initial state, restoring its resistance. Resistive strain sensors are particularly well-suited for soft robots with significant deformations due to their straightforward assembly process, convenient signal reading, high sensitivity, and wide operation strain range [31-33]. Anastasia Koivikko et al. [34] developed a curvature sensor for soft robotic devices using screen-printed silver conductors. This sensor is positioned on the inside surface of the soft robot near the limiting layer and has a limited measurement range of 2% strain with a sensitivity gauge factor (GF) of up to 7. Jun et al. [35] developed a high-stretchable strain sensor based on a carbon black-filled elastomer, which was fabricated using film-casting techniques and CO_2 laser ablation. This sensor improved the measurement range and operated under strains as high as 500% but possessed only 1.62–3.37GF in resistive mode. Saeb Mousavi et al. [36] improved the sensitivity of flexible sensors. They proposed an anisotropic resistive strain sensor that can be directly integrated into a soft robot to improve the sensitivity of flexible sensors. This design was fabricated by 3D printing using carbon-nanotube-reinforced polylactic acid (PLA-CNT). The sensitivity and anisotropy of the sensor can be adjusted by manipulating printing parameters. The sensitivity achieved a high value, but the breakage strain was below 20%. The simultaneous achievement of high sensitivity and wide measurement range in existing sensors remains challenging, which poses a significant obstacle to their application in soft robots.

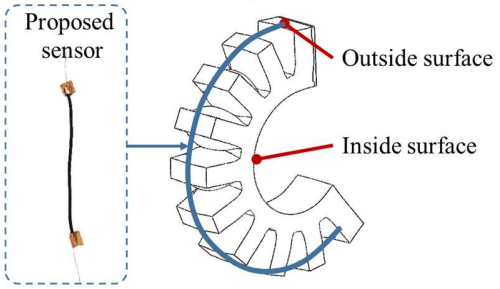

Fig. 1. Diagram of the inside and outside surfaces of the soft pneumatic gripper and the integrated proposed sensor.

To address these issues, a high-stretchable and flexible strain sensor based on the worm-surface-like microstructures has been proposed to achieve an extensive strain measurement range with a relatively high sensitivity. This sensor can be integrated into the outside surface of a soft pneumatic gripper for shape sensing, as shown in Fig. 1. When the soft pneumatic gripper grabs a target object, its outside surface generates the most significant deformation, providing an excellent sensing position for measurement. Meanwhile, integrating the strain sensor on the outside surface of the soft gripper can avoid unnecessary interferences with the target objects by its inside surface. The presented sensor comprises a viscoelastic fiber made of Ecoflex-10 and an outer conductive layer of Carbon Black (CB) powder. A 3D printing customized mold is utilized to generate the worm-surface-like microstructures for the presented sensor, providing a low-cost and convenient method. The produced worm-surface-like microstructures can enhance the surface area of the viscoelastic fibers and improve surface adhesion, reducing the sensor's initial resistance and enhancing conductive connectivity under large deformation. As a result, these advantages lead to a more stable sensing signal and improve the sensitivity. On the other hand, the designed microstructures effectively mitigate local strain on the surface of viscoelastic fibers, improving their stretchability and expanding the measurement range. Meanwhile, these microstructures can also reduce the required tension for achieving equivalent deformation, reducing the impact on the motion of the measured soft grippers. Adhesion energy tests and strain simulations have been conducted to validate and illustrate the design principles and advantages of the microstructures. Cyclic loading and unloading tests have been performed to characterize the mechanical and electrical performances of the sensor and investigate its tensile characteristics, hysteresis, and repeatability. The proposed sensor can be well applied to the outside surface of a soft pneumatic gripper with the merits of a large measurement range and high sensitivity. The accuracy of the curvature estimation is verified by grasping eight objects with different diameters, demonstrating the effectiveness of the soft pneumatic gripper integrated with the proposed sensor for the shape estimation of unknown objects.

II. Materials and Methods

A. Design Principle and Fabrication Process of the Proposed High-stretchable Strain Sensor

The proposed high-stretchable strain sensor consists of a central viscoelastic fiber (OD=2 mm) with worm-surface-like microstructures and an outside conductive layer, as shown in Fig. 2a). The central viscoelastic fiber is made of Ecoflex-10 silicone (America, Smooth-On, Inc.) with high stretchability and medium surface adhesion by a 3D printing customized mold. Its high stretchability enables the sensor to measure large deformations, and its medium surface adhesion is intended to adhere to the conductive layer so that the strain can be measured by electrical signals. The conductive layer consists of CB powder, which exhibits a broader measurement range and obtains a more stable electrical signal than other carbon-based

materials in the proposed sensor configuration. These advantages make it adaptable and applicable for strain measurement under large deformation.

The conductive layer of the proposed sensor consists of CB powder with interstitial spaces between the particles, as shown in Fig. 2b). When subjected to a tensile force, the viscoelastic fiber undergoes stretching which causes deformation of the outer conductive layer, leading to a reduction in density of CB powder and fewer conductive pathways being formed. Consequently, the sensor exhibits an increase in resistance R [37, 38], which can be quantitatively measured to reflect the strain experienced by the sensor. When the strain ε reaches a high level, the increase in the density change tends to plateau, making the rise in sensor resistance negligible. The presented worm-surface-like microstructures simultaneously enhance the surface area of the viscoelastic fiber, enhance surface adhesion, reduce the initial resistance of the sensor, and improve conductive connectivity during large deformations, thereby leading to enhanced signal stability. Consequently, this improvement in the worm-surface-like microstructures leads to improved sensitivity, according to the Equation for the gauge factor:

$$\mathrm{GF} = (\Delta R \,/\, R_0) \,/\, \varepsilon \qquad (1)$$

where ΔR denotes the change in resistance of the sensor. R_0 denotes the initial resistance, and ε denotes the strain. The designed microstructures are effective in reducing localized strain on the surface of viscoelastic fibers, thereby enhancing their tensile properties. Furthermore, the microstructures reduce the required tension for the same level of deformation, minimizing its impact on the motions of the measured objects.

The fabrication of the proposed high-stretchable strain sensor can be divided into three steps, as shown in Fig. 2a).

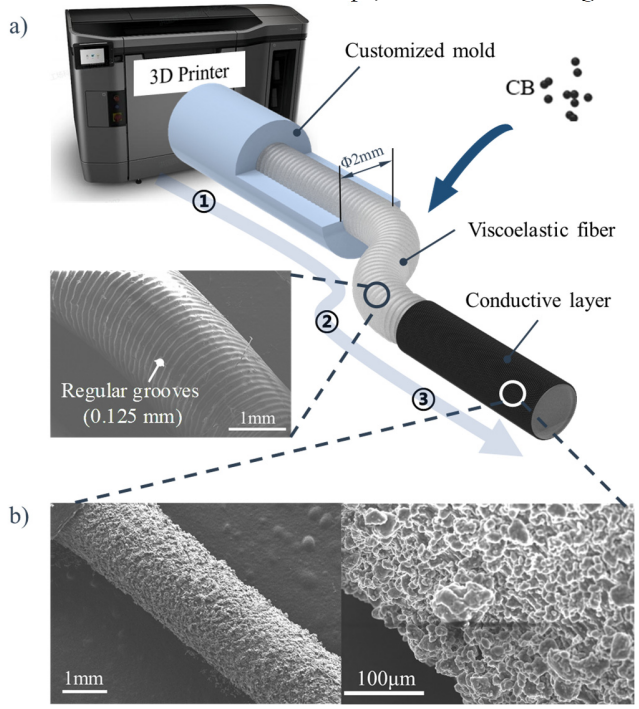

Fig. 2. The design principle and fabrication process of the proposed high-stretchable strain sensor. a) Fabrication process and worm-surface-like microstructures on the surface of viscoelastic fibers as observed by a scanning electron microscope (SEM); b) The proposed high-stretchable strain sensor observed by an SEM.

(1) The viscoelastic fiber with worm-surface-like microstructures was fabricated by infusion molding. After mixing part A and part B of silicone with a ratio of 1:1 by weight and stirring them thoroughly until homogeneous, the mixture was placed in a defoamer to extract air bubbles for 5 min. A syringe squeezed Such treated silicone into a customized 3D-printing mold (photosensitive resin material, Lite 600HD, Union Tech, CN). The worm-surface-like microstructures on the surface of the viscoelastic fiber are provided by such customized mold because the surface of the 3D-printed mold presents a regular arrangement of these microstructures produced by layer-by-layer photocuring. After maintaining room temperature for 4 hours to realize improved solidification, the formed viscoelastic fibers were removed from the mold. (2) Then, the fabricated viscoelastic fiber is placed in a sealed tank containing CB powder to be uniformly coated. (3) After that, the excess CB powder is removed to obtain the proposed high-stretchable strain sensor. Scanning electron microscopy (SEM) has observed the sensor microstructures, as shown in Fig. 2b).

The worm-surface-like microstructures shown in Fig. 2a) enhance the surface adhesion of the viscoelastic fiber, thereby augmenting the sensor's sensitivity under significant deformation. This is achieved by increasing the surface area and amplifying the inherent surface adhesion from the Ecoflex-10 silicone material [39]. In addition, reducing local strain on the surface of viscoelastic fibers by worm-surface-like microstructures can also improve the sensor's measurement range. When the strain exceeds the measurement range, this sensor may have viscoelastic fiber breakage, an open circuit of the conductive layer, or other failures. These worm-surface-like microstructures contribute to reducing local strain experienced by the viscoelastic fibers during stretching, thereby increasing the measurement range. Overall, the combination of enhanced surface adhesion and reduced local strain improves the presented sensor's performances in sensitivity and measurement range, making it more suitable for applications requiring high sensitivity and large deformation.

B. Performances Enhancement of High-stretchable Strain Sensors via worm-surface-like Microstructures

In order to verify the enhanced surface adhesion capacity and reduced local strain of the viscoelastic fiber in the high-stretchable strain sensors via worm-surface-like microstructures, the surface adhesion comparison test and local strain simulation were carried out.

1) *Enhanced Surface Adhesion on the Surface of Viscoelastic Fiber*

The surface adhesion comparison test was performed to verify the increase in surface adhesion by the worm-surface-like microstructures. Due to the curved nature of the viscoelastic fiber in the sensor, measuring surface adhesion force is challenging. Therefore, flake samples (10 mm×10 mm×2 mm) were fabricated to measure the upper surface adhesion with and without microstructures toward CB powder. The experimental illustration of the surface adhesion comparison test is shown in Fig. 3a). The samples with and without worm-surface-like microstructures were fixed on a tensile machine through slides, respectively. A thick tape

(3M™VHB™, US, 4910) attached to a stick by epoxy resin adhesive (Kafuter, CN, K-8818) was stuck to the surface of the sample. The force applied to the thick tape to peel off the upper surface of the samples with CB powder was provided and recorded by the tensile machine MTS Criterion (Model 42, MTS Systems Corporation). The peak peel force for the sample with and without worm-surface-like microstructures was 3.09 N and 1.52 N, respectively (Fig. 3b)). According to the sample's upper surface area of 100 mm^2, the adhesion energy for the surface of samples with and without worm-surface-like microstructures was 30.9 kPa and 15.2 kPa, respectively. These results demonstrate that the worm-surface-like microstructures can significantly improve the surface adhesion of the viscoelastic fiber utilized for the proposed high-stretchable strain sensor. When undergoing large deformation, the density change of carbon black powder on the surface of the sensor with microstructure is more significant than that of the sensor without microstructure. As a result, the presence of worm-surface-like microstructures can enhance the density change on this sensor surface during stretching. This increased density change leads to a higher resistivity change ΔR, enhancing the sensor's sensitivity (Equation (1)).

2) *Reduced Local Strain on the Surface of Viscoelastic Fiber*

To verify the improvement of worm-surface-like microstructures on the measurement range of the proposed high-stretchable strain sensor, strain simulations were performed for the fibrous models with and without worm-surface-like microstructures in Abaqus/CAE 2021. Based on the Yoeh model [40], the material parameters were configured, and the viscoelastic fibers were stretched to an overall strain of 300% from their initial length (Fig. 3c)). Paths were established along the axial direction on the model surface to capture the local strain distribution pattern on the surface of the viscoelastic fibers at 300% overall strain. As the strain increases, the local

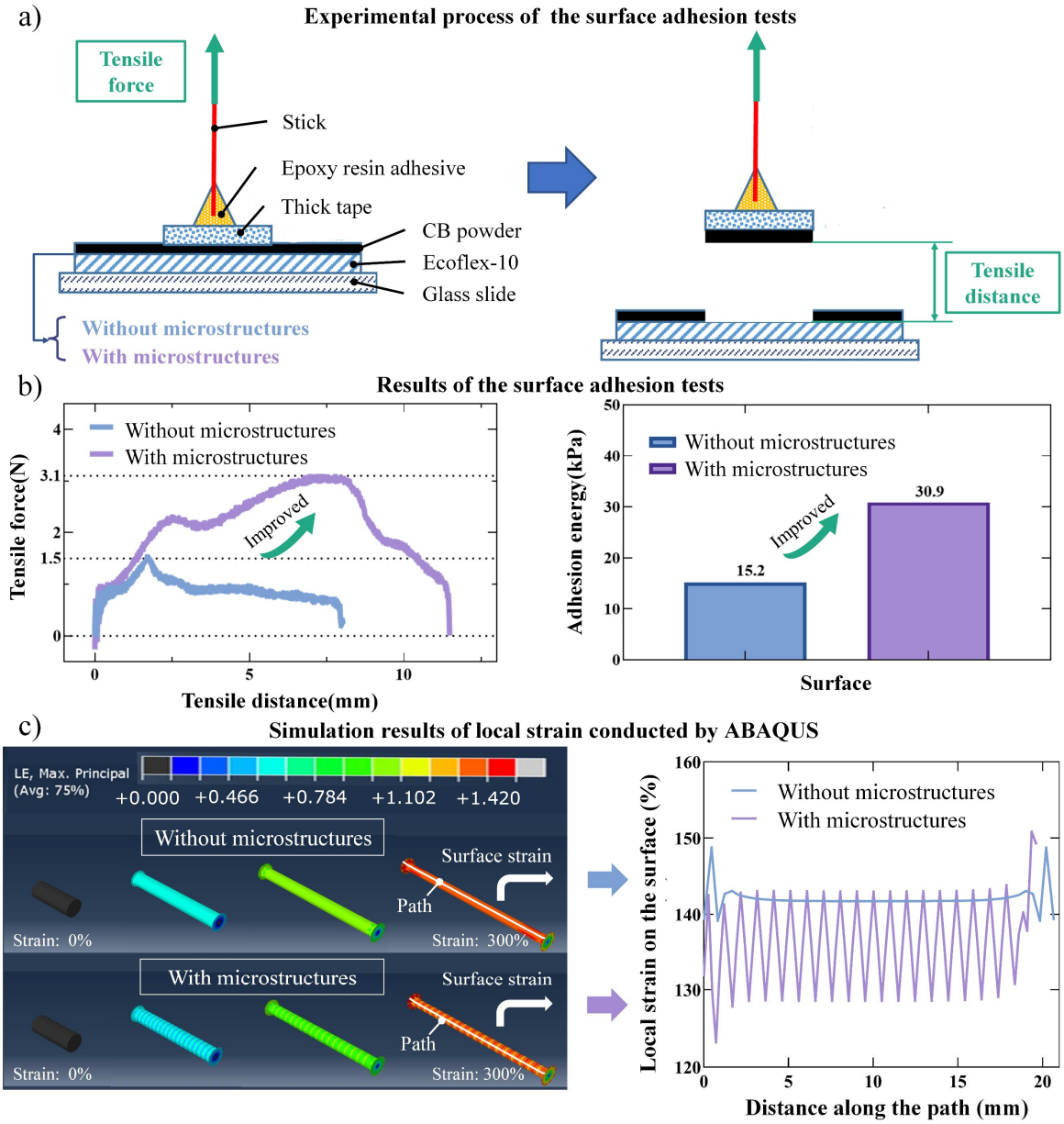

Fig. 3. Surface adhesion tests and strain simulation analysis by ABAQUS. a) Experimental process of the surface adhesion tests; b) Results of the surface adhesion tests; c) Simulation results of local strain conducted by ABAQUS.

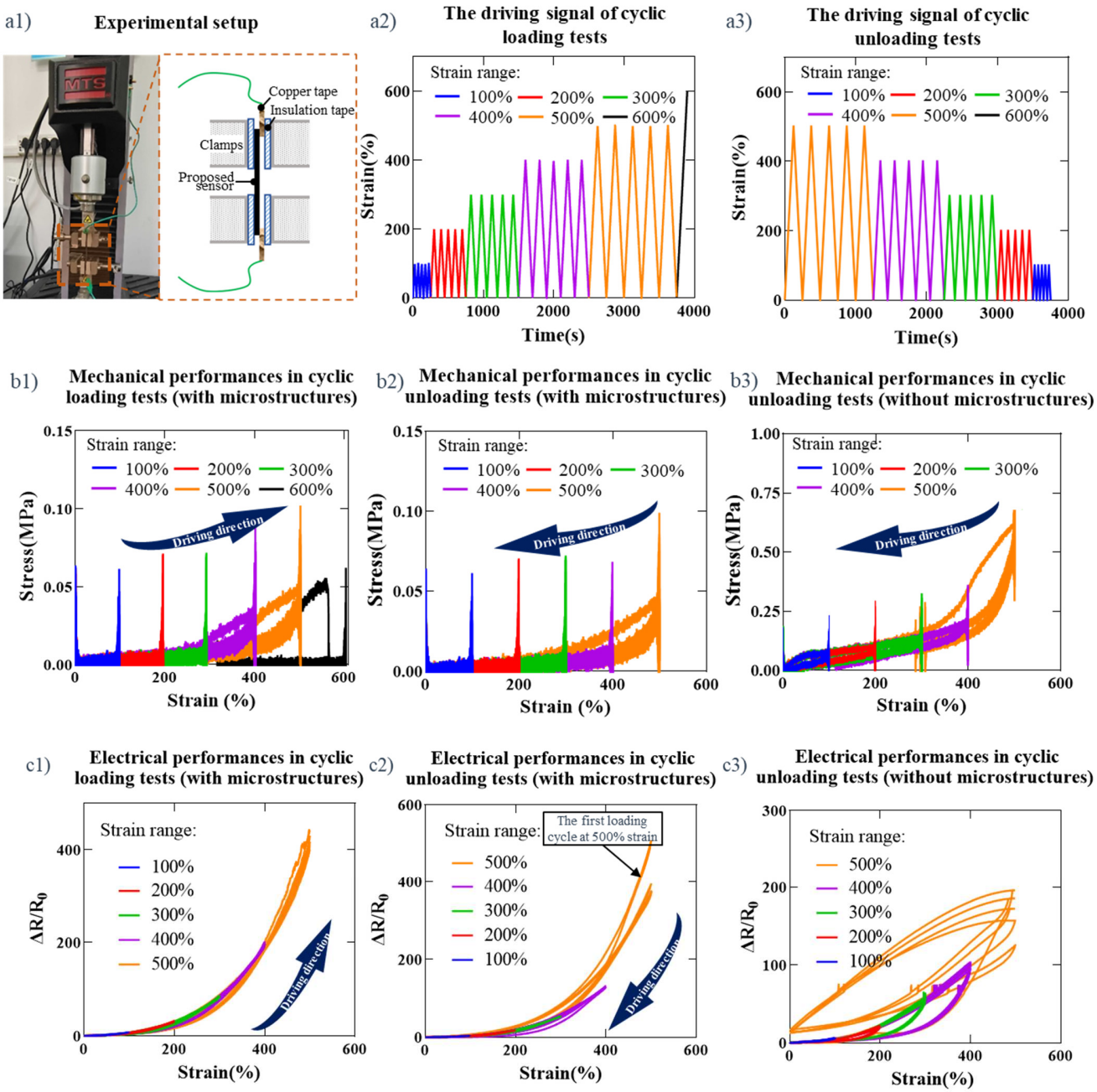

Fig. 4. Experimental setup and results of performance tests. a1) Experimental setup for performance tests; a2) The driving signal for cyclic loading tests; a3) The driving signal for cyclic unloading tests; b1) Mechanical performances of the proposed high-stretchable strain sensor with worm-surface-like microstructures via cyclic loading test; b2) Mechanical performances of this sensor with worm-surface-like microstructures via cyclic unloading test; b3) The mechanical performances of this sensor without worm-surface-like microstructures via cyclic unloading test; c1) The electrical performances of this sensor with worm-surface-like microstructures via cyclic loading test; c2) The electrical performances of this sensor with worm-surface-like microstructures via cyclic unloading test; c3) The electrical performances of this sensor without worm-surface-like microstructures via cyclic unloading test.

strain on the surface of viscoelastic fiber with worm-surface-like microstructures grows more slowly than that of viscoelastic fiber without worm-surface-like microstructures. At an overall strain of 300%, the local strain on the surface of viscoelastic fibers without worm-surface-like microstructures is approximately 142%. However, for viscoelastic fibers with worm-surface-like microstructures, the local strain on their surface ranges from 128% to 143%. Therefore, the worm-surface-like microstructures significantly reduce the local strain on the surface of viscoelastic fibers. These results demonstrate that under the same overall strain, the worm-surface-like microstructures can reduce the surface strain of viscoelastic fibers and increase the density of carbon material powder on the surface of viscoelastic fibers. As a result, the proposed strain sensor has higher stretchability and more stable circuit connection under the ultimate tensile state, thereby enhancing the sensor's measurement range.

III. Experiments and Results

A. Performance Tests of the Proposed High-stretchable Strain Sensor

The mechanical and electrical performances of the sensors with and without microstructures were tested and compared to investigate the impact of microstructures on sensor performances. The proposed high-stretchable strain sensor was mounted on a tensile machine MTS Criterion for performance tests (Fig. 4a1)). Each loading loop started from the original length (a strain of 0%), and the strain range of the loading loop increased or decreased with a strain step size of 100%. The cyclic loading tests demonstrate an increasing strain range, whereas the cyclic unloading tests exhibit a decreasing strain range. Each loading loop was repeated five times. The driving speed was set at 2mm/s, and the sampling frequency for the resistance was 100Hz. The cyclic loading and unloading tests' driving signals are shown in Fig. 4a2)-a3), respectively.

1) *Characterization of Mechanical Performances for the Proposed Strain Sensor*

The mechanical performances of the proposed high-stretchable strain sensor were investigated by conducting cyclic loading and unloading tests, aiming to explore the impact of its worm-surface-like microstructures. The tensile distance and force were recorded during the experiment, with the results of both the cyclic loading and unloading tests presented in Fig. 4b1)-b2), respectively. It can be seen from the results of the cyclic loading test that the degree of hysteresis increases significantly after the strain of viscoelastic fiber is beyond 300% and the viscoelastic fiber is broken at strain between 500% and 600%. Therefore, the maximum measurement strain of the proposed high-stretchable strain sensor does not exceed 600%. Furthermore, it has been observed from the results of the cyclic unloading test that the hysteresis of the viscoelastic fiber decreases significantly after large deformation, which is attributed to a weakening in stress relaxation of the viscoelastic material after its initial stretch to maximum capacity. In order to minimize the effect of stress relaxation, cyclic unloading tests were performed on the designed sensors without microstructures for comparison, and the results are illustrated in Fig. 4b3). It can be seen that under the same-level strain, the presented sensor design with worm-surface-like microstructures needs less stress. Therefore, the worm-surface-like microstructures can increase the sensor flexibility and reduce its impact on the motion of the object being measured.

2) *Characterization of Electrical Performances for the Proposed Strain Sensor*

To explore the proposed high-stretchable strain sensor's electrical performances, the worm-surface-like microstructures sensor was subjected to a cyclic loading and unloading test within the strain range of 0-500%. Each loading loop during these tests was repeated five times. The results of the first loading loop among the five loading loops at each strain are represented in dark colors, while the remaining four loading loops are represented in light colors. The results of cyclic loading and unloading tests are summarized in Fig. 4c1)-c2), respectively. The sensitivity of this sensor varies at different strains and increases as the strain increases (up to 206.6 for GF), so this sensor is more advantageous in high-strain situations. The relative resistance change value ($\Delta R/R_0$) of the proposed high-stretchable strain sensor has a significant hysteresis during the first loading because of the characteristic of stress relaxation. This hysteresis is mitigated after the first loading to the maximum strain level, and this sensor performance tends to stabilize.

To validate the enhanced strain sensitivity and measurement range offered by the worm-surface-like microstructures, the tensile experiments were conducted on the proposed strain sensors without the worm-surface-like microstructures made from viscoelastic fibers. The relative resistance change value with strain was recorded from 0% to 500% with 100% as the strain step size, as shown in Fig. 4c3). The hysteresis of the sensor without microstructures is more significant than that of the sensor with microstructures, and the sensor fails when the strain exceeds 400%. The sensor without microstructures reaches the maximum strain measurement of 400% strain, with a GF ranging from 5.27 to 26.19. On the other hand, the sensor with microstructures achieves the maximum strain measurement in the range of 500% to 600% strain, with a GF ranging from 7.40 to 206.60. Thus, it is evident that the sensor with worm-surface-like microstructures exhibits a wider measurement range and higher sensitivity under large deformation.

To explore the effect of speed on the electrical performances of the proposed high-stretchable strain sensor, the sensor was driven to the strain range of 300% at 2 mm/s, 5 mm/s, 10 mm/s, 20 mm/s, 40 mm/s, 80 mm/s, 100 mm/s, and 120 mm/s, and the tensile processes were repeated five times at each level of speed, as shown in Fig. 5. At the driving speed of 2 mm/s, the relative resistance change is 52.64, and the relative resistance change increases with the driving speed. Until the driving speed was 40 mm/s, the relative resistance change increased to 74.55. After that, the relative resistance change did not vary significantly and remained stable at around 76 as the driving speed increased to 120 mm/s. This lower relative resistance change at low-velocity driving is attributed to the stress relaxation of the viscoelastic fiber. The stress relaxation reduces the local strain on their surface and increases the density of CB powder on their surface, reducing the relative resistance change. Conversely, under lower driving speed conditions, insufficient stress relaxation time has little effect on relative resistance change. The proposed high-stretchable strain sensor achieves optimal sensitivity when driven at a minimum speed of 40 mm/s.

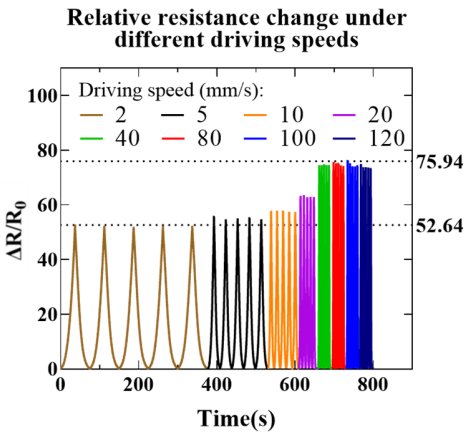

Fig. 5. Relative resistance change under different driving speed.

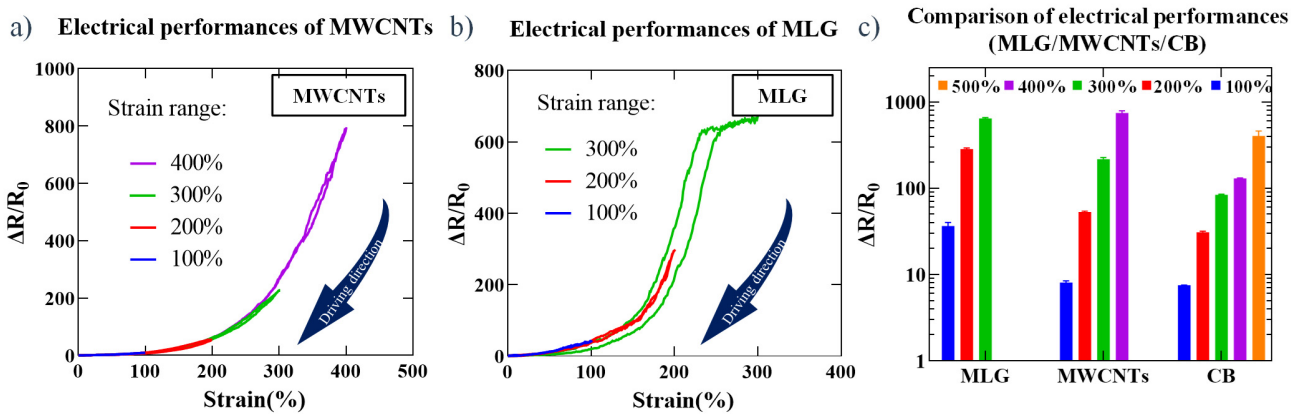

Fig. 6. Results of electrical performance tests and comparative analysis for sensors made with other carbon-based materials. a) Electrical performances of the sensor made of MWCNTs; b) Electrical performances of the sensor made of MLG; c) Comparison of performances characterization results of three sensors.

3) *Influences of Different Conductive Materials on the Proposed Strain Sensor*

To explore the influences of conductive materials on the performances of the proposed strain sensor, some other carbon-based materials (Multi-Walled Carbon Nanotubes and Multilayer Graphene) were utilized as conductive materials for sensor fabrication. Subsequent tensile experiments were conducted on these sensors. Both samples were subjected to the cyclic unloading test. The measurement range of Multi-Walled Carbon Nanotubes (MWCNTs) samples is from 0% to 400% strain. The curve for MWCNTs (Fig. 6a)) is more linear at a low strain range, but this curve's linearity decreases as the strain range increases. The sensitivity of sensors made from MWCNTs is higher than that of sensors made from CB (up to 206.6 for GF), with a maximum value of 673.1 for GF. The strain measurement range of the Multilayer Graphene (MLG) samples was less than 300%. Moreover, the relative resistance changes slowly rise after reaching the strain level of about 260%. The curve (Fig. 6b)) shows that the sensitivity of this sensor made of MLG increases with increasing strain (the maximum value of GF is 782.6).

To compare the hysteresis performances of the proposed sensors made of different conductive materials, the index γ_H [1] was applied to evaluate the hysteresis performances, as defined by Equation (2):

$$\gamma_H = \pm\frac{1}{2}\cdot\frac{\Delta H_{\max}}{\gamma_{FS}} \tag{2}$$

where $\Delta H_{\max}$ denotes the maximum resistance difference between cyclic loading and unloading at the same strain level and γ_{FS} denotes the resistance at full scale. The hysteresis performance results are summarized and compared in Table I. The hysteresis performances of sensors made from CB exhibit relatively stable behavior (3.02%-3.72%), with higher hysteresis under significant deformations compared with more minor deformations. Conversely, sensors fabricated from MWCNTs display lower hysteresis (3.24%) under larger deformations but higher hysteresis (5.82%) under smaller deformations. On the other hand, sensors made from MLG demonstrate the highest hysteresis(15.65%) under significant deformations compared to the other two groups of sensors.

The comparison between the measurement range and strain sensitivity of the proposed high-stretchable strain sensors made from the three carbon-based materials has been summarized and shown in Fig. 6c). The sensor's data signal made by CB material is stable and has an extensive measurement range with moderate sensitivity. The sensor made of MWCNTs has a moderate measurement range and sensitivity. The sensor made from MLG achieves the highest sensitivity, but the signal fluctuation is significant, and the measurement range is relatively limited. Therefore, this sensor made from MLG is more suitable for applications under low-strain usage conditions.

TABLE I
HYSTERESIS PERFORMANCES OF SENSORS MADE OF DIFFERENT CONDUCTIVE MATERIALS UNDER DIFFERENT STRAINS

Strain	CB	MWCNTs	MLG
100%	3.32%	5.82%	6.66%
200%	3.72%	6.12%	2.99%
300%	3.02%	3.12%	15.65%
400%	3.08%	3.24%	/
500%	3.44%	/	/

B. Curvature Radius Estimation for the Soft Pneumatic Gripper

1) *Experimental Setup for the Curvature Radius Estimation*

In order to verify the application potential of the proposed strain sensor in shape estimation for soft robots, a pneumatic soft gripper was designed and utilized for curvature radius estimation. The detailed experimental setup has been illustrated in Fig. 7. The hardware configuration comprises a PC, a microcontroller, a linear stage with a step motor, an air cylinder, an air pressure sensor, an LCR meter, a customized soft pneumatic gripper, and the prototyped sensor. The microcontroller (Arduino UNO) reads signals from the PC and controls the step motor. The step motor runs at 20 Hz to actuate the air cylinder (inner diameter =25 mm, length =150 mm) via the linear stage to drive the soft pneumatic gripper to bend. The air pressure sensor (PCM380, Suzhou Xuansheng Instrument Technology Ltd., Suzhou, CN) with a sensing accuracy of 10 Pa and an update rate of 20 Hz is employed to provide internal pressure data. The proposed strain sensor has been integrated into the outside surface of the soft pneumatic gripper to achieve curvature perception at different bending angles. Based on the assumption of constant curvature, more significant strain can be measured on the outside surface of the soft pneumatic gripper

under the same morphology. Thus, arranging sensors on the outside surface of the soft pneumatic gripper can improve the measurement resolution and make the experimental results more accurate. On the other hand, the utilized soft pneumatic gripper needs to interact with the captured objects through the inside surface. Therefore, the integration of the sensor on the outside surface of the soft pneumatic gripper does not affect its interaction with the captured objects. Subsequently, this strain sensor is connected to the LCR meter via two copper wires to measure its resistance during the gripper deflection.

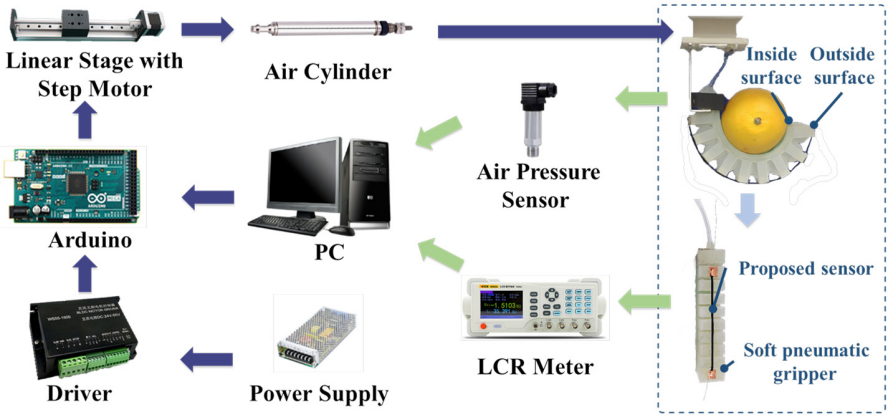

Fig. 7. Experimental setup for curvature estimation by a soft pneumatic gripper integrated with the proposed high-stretchable strain sensor.

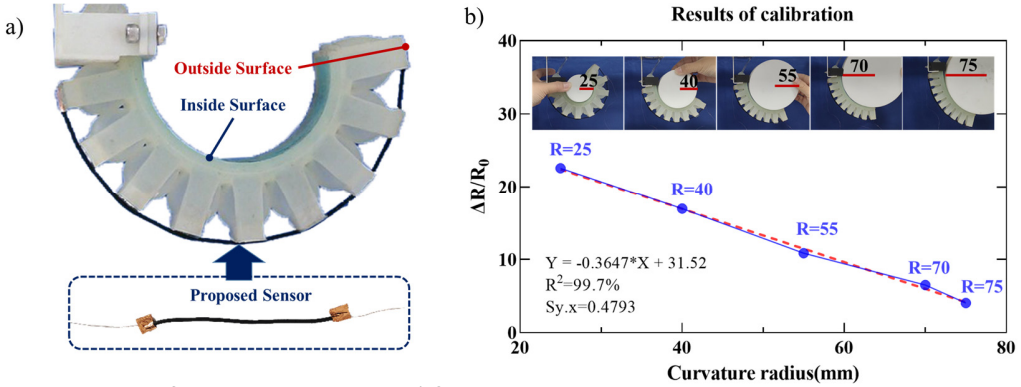

Fig. 8. a) Experimental illustration for grasping experiments; b) Calibration between the proposed sensor's relative resistance change and curvature radius.

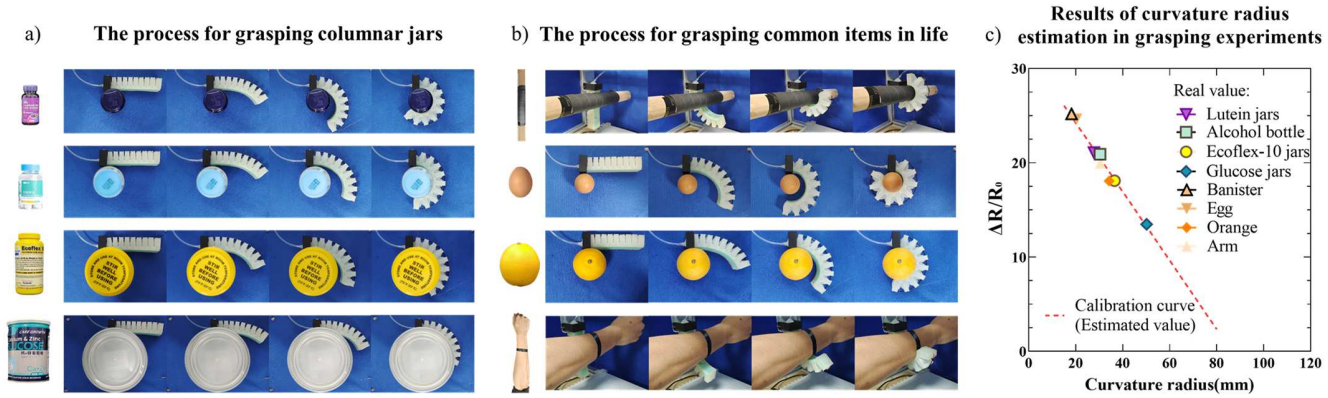

Fig. 9. Results of curvature radius estimation for the soft pneumatic gripper in grasping experiments. a) The process for grasping columnar jars with unknown diameter by a soft pneumatic gripper equipped with the proposed sensor on the outside surface; b) The process for grasping common items in life; c) Results of grasping experiments.

TABLE II
MEASUREMENT RESULTS AND ERRORS OF THE GRASPING EXPERIMENTS

Parameter	Columnar jars				Common items in life			
	Lutein jars	Alcohol bottle	Ecoflex-10 jars	Glucose jars	Banister	Egg	Orange	Arm
Real curvature radius (mm)	27.70	30.34	36.52	50.17	18.22	20.39	34.19	30.45
Relative resistance ($\Delta R/R_0$)	21.09	20.91	18.09	13.47	25.18	24.64	18.06	19.95
Estimated curvature radius (mm)	28.69	29.04	36.83	49.59	17.34	18.84	36.11	31.86
Relative error	3.57%	4.28%	0.85%	1.16%	4.83%	7.60%	5.62%	4.63%

2) *Calibration of the Proposed Strain Sensor for Curvature Radius Estimation*

Grasping experiments were performed to calibrate the proposed high-stretchable strain sensor and characterized, as shown in Fig. 8a). This sensor was calibrated with 5 discs of known curvature radius (25 mm, 40 mm, 55 mm, 70 mm, 75mm). When the soft pneumatic gripper bent to fit the outside surface of the measured objects, the corresponding resistance change values of the proposed strain sensor were recorded. The loading-unloading grasping experiments have been conducted, and the peak values in the variation curves are utilized to represent the different curvature radii of grasped objects. The relationship between the curvature radius of discs and the relative resistance change has been determined based on such grasping experiments for calibration. As illustrated in Fig. 8b), the blue points and their connecting lines represent the calibration results, while the red line denotes the fitting results for the calibrated data by simple linear regression. It can be found that the proposed strain sensor achieves an excellent linearity of 99.70% for the curvature radius estimation.

3) *Curvature Radius Estimation for the Soft Pneumatic Gripper in Grasping Experiments*

To further validate the curvature radius estimation capacity and accuracy, another four columnar jars of unknown curvature radius with different sizes, along with everyday items in life such as a railing, an egg, an orange, and a human arm, have been utilized in the grasping experiments. The grasping process of the soft pneumatic gripper is shown in Fig. 9a)-b), while the corresponding results are presented and summarized along with their errors in Fig. 9c) and Table II. The results show that the relative error in curvature estimation for regular columnar jars (average error of 2.47%) is smaller than the relative error in curvature estimation for common items in life (average error of 5.67%). This is attributed to surface softness, uneven curvature, or tiny curvature radius in common items in life. The error in grasping experiments is significantly reduced compared with the estimation of curvature radius in free space, as the soft pneumatics gripper's constant curvature performance can be enhanced by conforming it to the surface of the object being grasped. Such results demonstrate the potential of the soft pneumatic gripper integrated with the proposed strain sensor for curvature estimation of objects through grasping experiments.

C. Discussion

The comparison of the performances between this work and other existing strain sensors [10, 15-17, 34-36, 41-44] has been summarized in Table III. Due to the limited tensile properties of glass materials, the measurement range and sensitivity of optical fiber sensors are typically low. Capacitive sensors improve the measurement range to some extent, but their sensitivity is still low when measuring tensile strain. For resistive sensors, most flexible resistive strain sensors encounter challenges in achieving a balance between sensitivity and measurement range. The reference in [42] achieves a GF of more than 5000, but the measurement range of only 20%. In contrast, the reference in [10] demonstrates the measurement range of 400%, but the GF is as low as 0.5-1. The proposed high-stretchable strain sensor in this paper achieves a maximum GF of 782.6 at a strain measurement range of 300% (for the sensor made of MLG) and a maximum GF of 206.6 at a strain measurement range of 500% (for the sensor made of CB) while taking into account both the measurement range and sensitivity. The proposed high-stretchable strain sensor exhibits greater sensitivity under large deformations, rendering its high sensitivity more effectively utilized without interfering with the motion of the soft pneumatic gripper when mounted on its

TABLE III
COMPARISON OF THE PERFORMANCES BETWEEN THIS WORK AND OTHER STRAIN SENSORS

Method		GF	Strain	Integrated object	Ref.
Sensing transducers	**Key materials**				
Optical	Fiber Bragg Grating	0.02	< 2.5%	Soft pneumatic gripper	Hao et al. [41]
Capacitive	Shieldex M-130 + Ecoflex	1.23	100%	Glove	Atalay et al. [17]
	CNT[a)]+PDMS[b)]	1	100%	Glove	Le et al. [16]
	Poly-aniline	2	20%	Glove	Kollosche et al. [15]
Resistive	CNT+ Dragonskin	0.5-1	400%	Soft pneumatic gripper	Liu et al. [10]
	Silver nanoink+ silicone	> 5000	> 20%	Glove	Yeo et al. [42]
	Silver ink+ TPU[c)]	7	2%	Soft robot	Koivikko et al. [34]
	PLA[d)]+ CNT	1342	<20%	Soft pneumatic gripper	Mousavi et al. [36]
	CB+ Ecoflex	1.62-3.37	500%	Glove	Jun et al. [35]
	Dielectric photopolymer	~ 35	0.2%	Soft robot	Shih et al. [43]
	Ecoflex+ Dragonskin+ Metallic inlets	~0.7–1	300%	Soft robot	Koivikko et al. [44]
	MLG/MWCNTs/ CB+ Ecoflex	782.6 (MLG) 673.1 (MWCNTs) 206.6 (CB)	< 300% (MLG) 400% (MWCNTs) 500% (CB)	Soft pneumatic gripper	This paper

[a)] Carbon Nanotube; [b)] Polydimethylsiloxane; [c)] Thermoplastic Polyurethane; [d)] Polylactic acid.

outside surface. Additionally, the designed microstructures yield enhanced flexibility upon the sensor and minimize its impacts on the motion of the soft pneumatic gripper during experimentation. The results of curvature estimation in the soft pneumatic gripper by the proposed high-stretchable strain sensor demonstrate its feasibility for shape sensing in soft robots.

The proposed sensor offers advantages in terms of a simple manufacturing method, low cost, and easy integration while demonstrating a wide measurement range and high sensitivity performances. However, simple manufacturing methods are insufficient for achieving process standardization, and manual operations may lead to unpredictable effects on sensor performances. Therefore, it is essential to select sensors from the same processing batch for performance characterization and curvature estimation experiments in order to mitigate the impact of manual manufacturing errors. Furthermore, the microstructure parameters can be further adjusted by other high-precision 3D-printing technologies (e.g. projection micro stereolithography) to customize the sensitivity and measurement range of the designed sensor to adapt to different application scenarios [45].

IV. Conclusions

This work proposes a novel high-stretchable strain sensor that mainly consists of a viscoelastic fiber with worm-surface-like microstructures and an outer conductive layer made of CB. The presented strain sensor achieves a wide range of measurements and a relatively high sensitivity due to the adoption of the designed microstructures. The microstructures on the sensor's surface are fabricated via a customized 3D-printing mold, which is a cost-effective and straightforward method. The introduction of the microstructures augments the surface area of viscoelastic fibers and enhances surface adhesion, thereby improving the sensitivity and the stability of circuit connection in the extremely stretched state. Furthermore, the microstructures lead to an enhancement of the fibers' stretchability and a notable extension of the sensor's measurement range. The electrical and mechanical performances of the proposed high-stretchable strain sensors have been characterized by cyclic loading and unloading experiments. The experimental results demonstrated high sensitivity and a wide measurement range of the proposed strain sensor. Besides, this presented strain sensor has been integrated with the soft pneumatic gripper to estimate the curvature radius of the grasped objects, validating the effectiveness of the proposed strain sensor for curvature estimation of a soft gripper. In future work, multi-modal sensing information and neural network algorithms will be introduced to realize accurate perception of complex and non-constant curvature properties of soft robots [41, 46]. Moreover, the closed-loop control method incorporating feedback from curvature information will be further investigated. In addition, the contact force sensor based on fiber Bragg grating (FBG) sensing technology will be integrated into the inside surface of the soft pneumatic gripper to realize the contact force detection during the interaction process [47, 48].

References

[1] S. I. Rich, R. J. Wood, and C. Majidi, “Untethered soft robotics,” *Nature Electronics,* vol. 1, no. 2, pp. 102-112, 2018.

[2] J. Shintake, V. Cacucciolo, D. Floreano, and H. Shea, “Soft Robotic Grippers,” *Advanced Materials,* vol. 30, no. 29, pp. 1707035, 2018.

[3] M. Amjadi, K. U. Kyung, I. Park, and M. Sitti, “Stretchable, skin-mountable, and wearable strain sensors and their potential applications: a review,” *Advanced Functional Materials,* vol. 26, no. 11, pp. 1678-1698, 2016.

[4] L. Ge, F. Chen, D. Wang, Y. Zhang, D. Han, T. Wang, and G. Gu, “Design, Modeling, and Evaluation of Fabric-Based Pneumatic Actuators for Soft Wearable Assistive Gloves,” *Soft Robotics*, 2020.

[5] A. Diodato, M. Brancadoro, G. De Rossi, H. Abidi, D. Dall’Alba, R. Muradore, G. Ciuti, P. Fiorini, A. Menciassi, and M. Cianchetti, “Soft robotic manipulator for improving dexterity in minimally invasive surgery,” *Surgical innovation,* vol. 25, no. 1, pp. 69-76, 2018.

[6] J. Guo, J. Low, X. Liang, J. S. Lee, Y. Wong, and R. C. H. Yeow, “A Hybrid Soft Robotic Surgical Gripper System for Delicate Nerve Manipulation in Digital Nerve Repair Surgery,” *IEEE/ASME Transactions on Mechatronics,* vol. 24, no. 4, pp. 1440-1451, 2019.

[7] R. Deimel, and O. Brock, “A novel type of compliant and underactuated robotic hand for dexterous grasping,” *INTERNATIONAL JOURNAL OF ROBOTICS RESEARCH,* vol. 35, no. 1-3, pp. 161-185, JAN-MAR, 2016.

[8] J. Zhou, X. Chen, U. Chang, Y. Liu, Y. Chen, and Z. Wang, "A Grasping Component Mapping Approach for Soft Robotic End-Effector Control." pp. 650-655.

[9] H. Wang, M. Totaro, and L. Beccai, “Toward perceptive soft robots: Progress and challenges,” *Advanced Science,* vol. 5, no. 9, pp. 1800541, 2018.

[10] R. Liu, S. Wang, H. Yang, and C. Shi, “Highly Stretchable Strain Sensor With Spiral Fiber for Curvature Sensing of a Soft Pneumatic Gripper,” *IEEE Sensors Journal,* vol. 21, no. 21, pp. 23880-23888, 2021.

[11] G. I. Hay, P. S. A. Evans, D. J. Harrison, D. Southee, G. Simpson, and P. M. Harrey, “Characterization of lithographically printed resistive strain gauges,” *IEEE Sensors Journal,* vol. 5, no. 5, pp. 864-871, 2005.

[12] E. Copertaro, “Assessment of resistive strain gauges measurement performances in experimental modal analysis and their application to the diagnostics of abrasive waterjet cutting machinery,” *Measurement,* vol. 188, pp. 110626, 2022.

[13] J. Guo, M. Niu, and C. J. O. Yang, “Highly flexible and stretchable optical strain sensing for human motion detection,” *Optica,* vol. 4, no. 10, pp. 1285-1288, 2017.

[14] M. Amanzadeh, S. M. Aminossadati, M. S. Kizil, and A. D. J. M. Rakić, “Recent developments in fibre optic shape sensing,” *Measurement,* vol. 128, pp. 119-137, 2018.

[15] M. Kollosche, H. Stoyanov, S. Laflamme, and G. Kofod, “Strongly enhanced sensitivity in elastic capacitive strain sensors,” *Journal of Materials Chemistry,* vol. 21, no. 23, pp. 8292-8294, 2011.

[16] C. Le, L. Song, P. Luan, Q. Zhang, N. Zhang, Q. Gao, D. Zhao, X. Zhang, M. Tu, F. Yang, W. Zhou, Q. Fan, J. Luo, W. Zhou, P. M. Ajayan, and S. Xie, “Correction: Corrigendum: Super-stretchable, Transparent Carbon Nanotube-Based Capacitive Strain Sensors for Human Motion Detection,” *Scientific Reports,* vol. 3, no. 1, pp. 3402, 2013.

[17] A. Atalay, V. Sanchez, O. Atalay, D. M. Vogt, F. Haufe, R. J. Wood, and C. J. Walsh, “Batch Fabrication of Customizable Silicone-Textile Composite Capacitive Strain Sensors for Human Motion Tracking,” *Advanced Materials Technologies,* vol. 2, no. 9, pp. 1700136, 2017.

[18] W. Hao, J. Guo, C. Wang, S. Wang, and C. Shi, “A Novel Capacitive-Based Flexible Pressure Sensor Based on Stretchable Composite Electrodes and a Dielectric Elastomer With Microstructures,” *IEEE Access,* vol. 8, pp. 142810-142818, 2020.

[19] Z. Guo, J. Xu, Y. Chen, Z. Guo, P. Yu, Y. Liu, and J. Zhao, “High-sensitive and stretchable resistive strain gauges: Parametric design and DIW fabrication,” *Composite Structures,* vol. 223, pp. 110955, 2019.

[20] W. Li, Y. Zhou, Y. Wang, Y. Li, L. Jiang, J. Ma, and S. Chen, “Highly Stretchable and Sensitive SBS/Graphene Composite Fiber for Strain Sensors,” *Macromolecular Materials and Engineering,* vol. 305, no. 3, pp. 1900736, 2020.

[21] G. Olson, C. Davies, G. S. Gupta, R. Davies, and L. Fullard, "Resistance measurements of polydimethylsiloxane (PDMS) stretch-sensors embedded with a conductive gel." pp. 1-5.

[22] Y. Peng, X. Wang, L. Zhong, K. Pang, Y. Chen, M. Wang, and W. Liu, “A Flexible Dual-Modal Sensing System for Synchronous Pressure and

Inertial Monitoring of Finger Movement," *IEEE Sensors Journal,* vol. 21, no. 9, pp. 10483-10490, 2021.
[23] C. Shi, X. Luo, P. Qi, T. Li, S. Song, Z. Najdovski, T. Fukuda, and H. Ren, "Shape Sensing Techniques for Continuum Robots in Minimally Invasive Surgery: A Survey," *IEEE Transactions on Biomedical Engineering,* vol. 64, no. 8, pp. 1665-1678, 2017.
[24] C. Shi, X. Luo, J. Guo, Z. Najdovski, T. Fukuda, and H. Ren, "Three-Dimensional Intravascular Reconstruction Techniques Based on Intravascular Ultrasound: A Technical Review," *IEEE Journal of Biomedical and Health Informatics,* vol. 22, no. 3, pp. 806-817, 2018.
[25] P. P. Wang, S. Q. Zhang, Z. Y. Liu, Y. X. Huang, J. Huang, X. M. Huang, J. Chen, B. M. Fang, and D. X. Peng, "Smart laparoscopic grasper integrated with fiber Bragg grating based tactile sensor for real-time force feedback," *Journal of Biophotonics,* vol. 15, no. 5, pp. 11, May, 2022.
[26] C. Shi, Z. Tang, and S. Wang, "Design and Experimental Validation of a Fiber Bragg Grating-Enabled Force Sensor With an Ortho-Planar Spring-Based Flexure for Surgical Needle Insertion," *IEEE Transactions on Medical Robotics and Bionics,* vol. 3, no. 2, pp. 362-371, 2021.
[27] D. Kwon, T.-I. Lee, J. Shim, S. Ryu, M. S. Kim, S. Kim, T.-S. Kim, and I. Park, "Highly sensitive, flexible, and wearable pressure sensor based on a giant piezocapacitive effect of three-dimensional microporous elastomeric dielectric layer," *ACS applied materials interfaces,* vol. 8, no. 26, pp. 16922-16931, 2016.
[28] F. Huang, J. Hu, and X. Yan, "Review of Fiber- or Yarn-Based Wearable Resistive Strain Sensors: Structural Design, Fabrication Technologies and Applications," *Textiles,* vol. 2, no. 1, pp. 81-111, 2022.
[29] Y. Peng, J. Wang, X. Tian, T. Liu, W. Geng, and Z. Zhu, "An Electronic Skin Strain Sensor for Adaptive Angle Calculation," *IEEE Sensors Journal,* vol. 22, no. 13, pp. 12629-12636, 2022.
[30] Y. Peng, J. Wang, K. Pang, W. Liu, J. Meng, and B. Li, "A Physiology-Based Flexible Strap Sensor for Gesture Recognition by Sensing Tendon Deformation," *IEEE Sensors Journal,* vol. 21, no. 7, pp. 9449-9456, 2021.
[31] R. Rahimi, M. Ochoa, W. Yu, and B. Ziaie, "Highly Stretchable and Sensitive Unidirectional Strain Sensor via Laser Carbonization," *ACS Applied Materials & Interfaces,* vol. 7, no. 8, pp. 4463-4470, 2015.
[32] E. Roh, B.-U. Hwang, D. Kim, B.-Y. Kim, and N.-E. Lee, "Stretchable, Transparent, Ultrasensitive, and Patchable Strain Sensor for Human–Machine Interfaces Comprising a Nanohybrid of Carbon Nanotubes and Conductive Elastomers," *ACS Nano,* vol. 9, no. 6, pp. 6252-6261, 2015.
[33] X. Liao, Z. Zhang, Z. Kang, F. Gao, Q. Liao, and Y. Zhang, "Ultrasensitive and stretchable resistive strain sensors designed for wearable electronics," *Materials Horizons,* vol. 4, no. 3, pp. 502-510, 2017.
[34] A. Koivikko, E. S. Raei, M. Mosallaei, M. Mäntysalo, and V. Sariola, "Screen-Printed Curvature Sensors for Soft Robots," *IEEE Sensors Journal,* vol. 18, no. 1, pp. 223-230, 2018.
[35] J. Shintake, Y. Piskarev, S. H. Jeong, and D. Floreano, "Ultrastretchable Strain Sensors Using Carbon Black-Filled Elastomer Composites and Comparison of Capacitive Versus Resistive Sensors," *Advanced Materials Technologies,* vol. 3, no. 3, pp. 1700284, 2018.
[36] S. Mousavi, D. Howard, F. Zhang, J. Leng, and C. H. Wang, "Direct 3D Printing of Highly Anisotropic, Flexible, Constriction-Resistive Sensors for Multidirectional Proprioception in Soft Robots," *ACS Applied Materials & Interfaces,* vol. 12, no. 13, pp. 15631-15643, 2020.
[37] J.-F. Zhang, Q. Zheng, Y.-Q. Yang, and X.-S. Yi, "High-density polyethylene/carbon black conductive composites. I. Effect of CB surface modification on its resistivity–temperature behavior," *Journal of Applied Polymer Science,* vol. 83, no. 14, pp. 3112-3116, 2002.
[38] W. Luheng, D. Tianhuai, and W. Peng, "Influence of carbon black concentration on piezoresistivity for carbon-black-filled silicone rubber composite," *Carbon,* vol. 47, no. 14, pp. 3151-3157, 2009.
[39] K. Emre, and S. N. Gorb, "Bioinspired further enhanced dry adhesive by the combined effect of the microstructure and surface free energy increase," *Acs Applied Materials & Interfaces*, pp. acsami.8b06686-, 2018.
[40] L. Marechal, P. Balland, L. Lindenroth, F. Petrou, C. Kontovounisios, and F. Bello, "Toward a common framework and database of materials for soft robotics," *Soft robotics,* vol. 8, no. 3, pp. 284-297, 2021.
[41] J. Hao, Z. Zhang, S. Wang, and C. Shi, "2D Shape Estimation of a Pneumatic-Driven Soft Finger with a Large Bending Angle Based on Learning from Two Sensing Modalities," *Advanced Intelligent Systems,* vol. 5, no. 10, pp. 2200324.
[42] J. C. Yeo, H. K. Yap, W. Xi, Z. Wang, C.-H. Yeow, and C. T. Lim, "Flexible and Stretchable Strain Sensing Actuator for Wearable Soft Robotic Applications," *Advanced Materials Technologies,* vol. 1, no. 3, pp. 1600018, 2016.
[43] B. Shih, C. Christianson, K. Gillespie, S. Lee, J. Mayeda, Z. Huo, and M. T. Tolley, "Design considerations for 3D printed, soft, multimaterial resistive sensors for soft robotics," *Frontiers in Robotics and AI,* vol. 6, pp. 30, 2019.
[44] A. Koivikko, V. Lampinen, M. Pihlajamäki, K. Yiannacou, V. Sharma, and V. Sariola, "Integrated stretchable pneumatic strain gauges for electronics-free soft robots," *Communications Engineering,* vol. 1, no. 1, pp. 14, 2022.
[45] Q. Ge, Z. Li, Z. Wang, K. Kowsari, W. Zhang, X. He, J. Zhou, and N. X. Fang, "Projection micro stereolithography based 3D printing and its applications," *International Journal of Extreme Manufacturing,* vol. 2, no. 2, pp. 022004, 2020.
[46] J. Hao, D. Song, C. Hu, and C. Shi, "Two-Dimensional Shape and Distal Force Estimation for the Continuum Robot Based on Learning From the Proximal Sensors," *IEEE Sensors Journal,* vol. 23, no. 10, pp. 10836-10846, 2023.
[47] K. Sun, M. Li, S. Wang, G. Zhang, H. Liu, and C. Shi, "Development of a Fiber Bragg Grating-Enabled Clamping Force Sensor Integrated on a Grasper for Laparoscopic Surgery," *IEEE Sensors Journal,* vol. 21, no. 15, pp. 16681-16690, 2021.
[48] Z. Tang, S. Wang, M. Li, and C. Shi, "Development of a Distal Tri-Axial Force Sensor for Minimally Invasive Surgical Palpation," *IEEE Transactions on Medical Robotics and Bionics,* vol. 4, no. 1, pp. 145-155, 2022.